Journal of Catalysis **189,** 247–252 (2000)
Article ID jcat.1999.2702, available online at http://www.idealibrary.com on IDEAL®

RESEARCH NOTE

Reactivity of $Rh^+(CO)_2$ during the NO–CO and CO–O_2 Reactions over Rh/Al_2O_3

Khalid A. Almusaiteer, Steven S. C. Chuang,[1] and Cher-Dip Tan

Department of Chemical Engineering, The University of Akron, Akron, Ohio 44325-3906

Received July 20, 1999; revised September 27, 1999; accepted September 28, 1999

Exposure of $Rh^+(CO)_2$ on Rh/Al_2O_3 to NO causes CO desorption and adsorption of NO as Rh–NO^+; exposure of $Rh^+(CO)_2$ to NO/H_2 produced N_2O at 573 K. The presence of both reductant (i.e., CO) and oxidant (i.e., NO or O_2) in the reactant pulse is needed to initiate and sustain the NO–CO redox reaction cycle for CO_2 formation.

Key Words: **gem-dicarbonyl; NO–CO reaction; Rh catalyst; adsorbed CO; transient studies; reactivity; redox cycle; adsorbed NO; infrared spectroscopy; mass spectrometry; oxidative disruption; reductive agglomeration; reaction mechanism.**

INTRODUCTION

The nature of sites associated with $Rh^+(CO)_2$, rhodium gem-dicarbonyl, and the mechanism of its formation have been subjects of extensive studies (1–20) because of fundamental interests in understanding the role of Rh surface states and their adsorbates in automobile catalysis (21–25). $Rh^+(CO)_2$ can be produced from CO adsorption on the oxide-supported Rh crystallites, oxidized Rh, $RhCl_3$, $Rh(NO_3)_3$, and partially decomposed Rh carbonyls (2, 9, 16, 19, 26–30). $Rh^+(CO)_2$ has been found to be a major CO adsorbate on the Al_2O_3- and SiO_2-supported Rh catalysts during the NO–CO and CO–O_2 reactions (5, 7, 9, 10, 17).

We have attempted to address the role and reactivity of $Rh^+(CO)_2$ in the NO–CO reaction by *in situ* infrared (IR) coupled with various transient techniques (16, 17, 28–32). *In situ* IR coupled with steady-state isotopic transient kinetic analysis (SSITKA) revealed a rapid exchange between gaseous ^{13}CO and $Rh^+(^{12}CO)_2$, but failed to provide unambiguous information to determine the role of $Rh^+(CO)_2$ in the reaction (31). The selective enhancement/poisoning technique, which we recently developed, has unambiguously identified Pd^0–NO and Pd^0–CO as active adsorbates for the NO–CO reaction on Pd/Al_2O_3 (33). The use of this technique on Rh/Al_2O_3 did not lead to useful information to determine the $Rh^+(CO)_2$ role in the NO–CO reaction due to extensive modification of the Rh catalyst surface state during the addition of O_2 as a poison (35).

In the present study, we have examined the $Rh^+(CO)_2$ reactivity and its role in CO_2 formation by exposing $Rh^+(CO)_2$ to NO, ^{13}CO/NO, NO/H_2, air, and ^{13}CO/air. Direct IR spectroscopic evidence is obtained to show involvement of $Rh^+(CO)_2$ in CO_2 formation during the ^{13}CO/NO pulse reaction over Rh/Al_2O_3.

EXPERIMENTAL

The 2 wt% Rh/Al_2O_3 and 0.2 wt% Rh/Al_2O_3 catalysts were prepared by incipient wetness impregnation of $RhCl_3 \cdot 2H_2O$ (Alfa Chemicals) onto a γ-alumina support (Alfa Chemicals, 100 m^2/g). The catalysts were dried overnight in air at room temperature and calcined by flowing air at 723 K for 6 h and then reduced by flowing H_2 at 723 K for 6 h. The dispersion of metal crystallite on Al_2O_3 was determined to be 9% for 2 wt% Rh/Al_2O_3 and 94% for 0.2 wt% Rh/Al_2O_3 by H_2 pulse chemisorption at 300 K.

Details of the experimental apparatus have been described elsewhere (34) and will be briefly discussed here. The experimental system consists of (i) the gas flow system with a GC six-port sampling valve and mass flow controllers for the NO, ^{12}CO, ^{13}CO, air, H_2, and He flow, (ii) the *in situ* IR reactor cell with self-supporting catalyst disk, and (iii) the analysis section with a Nicolet Magna 550 IR spectrometer for recording IR spectra of adsorbed species and Balzers QMG 112 quadruple mass spectrometer (MS) for the analysis of reactants and products. The gaseous responses for m/e ratios corresponding to $m/e = 28$ (^{12}CO and N_2), $m/e = 29$ (^{13}CO), $m/e = 30$ (NO), $m/e = 44$ ($^{12}CO_2$ and N_2O), and $m/e = 45$ ($^{13}CO_2$) were monitored by the MS. The CO_2 and N_2O ($m/e = 44$) responses were separated by using the response ratio of the CO_2^+ ($m/e = 44$) primary ionization and the CO_2^{++} ($m/e = 22$) double ionization.

[1] To whom correspondence should be addressed. E-mail: schuang@uakron.edu.

0021-9517/00 $35.00

RESULTS AND DISCUSSION

Formation of $Rh^+(CO)_2$

In situ IR studies have shown that CO adsorbs as gem-dicarbonyl [$Rh^+(CO)_2$], linear CO [Rh^0–CO], and bridged CO [Rh_2^0–CO] on supported Rh catalysts (1–20, 29–31). The concentration of each species on the Rh surface is governed by the oxidation state of the Rh surface which depends on the Rh crystallite size, redox environment (i.e., NO/CO ratio), and reaction temperature (1–20, 28–32). Small Rh crystallites, high NO/CO ratio, and low temperature (i.e., below the light-off temperature) favor the $Rh^+(CO)_2$ formation and vice versa for large Rh crystallites (7).

Attempts to study the reactivity of preadsorbed Rh^0–CO and $(Rh)_2$–CO toward gaseous NO at temperatures above 473 K have failed due to its rapid desorption (16). It should be noted that desorption of Rh^0–CO at 573 K in the present study was due to its low thermal stability rather than its reaction with oxygen impurities in He flow. Potential oxygen impurities in He flow was verified by flowing He over a reduced Rh/Al_2O_3 bed/containing adsorbed CO before entering the IR reactor cell. Rh^0–CO and $(Rh)_2$–CO in the IR reactor cell was flushed by He and no CO_2 was observed.

$Rh^+(CO)_2$ produced from the NO–CO reaction persisted in He flow at temperatures as high as 633 K on 0.2 wt% Rh/Al_2O_3 (32). To facilitate Rh^+ formation, the prereduced 2 wt% Rh/Al_2O_3 and 0.2 wt% Rh/Al_2O_3 were oxidized by flowing NO which has been shown to be effective in facilitating the oxidative disruption of Rh^0 crystallites to isolated Rh^+ sites (19). Flowing CO over the NO-pretreated catalyst at 573 K produced $Rh^+(CO)_2$.

Reaction of $Rh^+(CO)_2$ with NO

Figure 1a illustrates the experimental approach involving a 1-cm^3 NO pulse over $Rh^+(CO)_2$ on 2 wt% Rh/Al_2O_3. Figures 1b and 1c show the IR spectra of adsorbates and MS analysis of the IR reactor cell effluent during a 1-cm^3 NO pulse over $Rh^+(CO)_2$ on 2 wt% Rh/Al_2O_3 at 573 K. Pulsing NO over $Rh^+(CO)_2$ produced cationic NO [Rh–NO^+] at 1910 cm^{-1} and dinitrosyl [$Rh^+(CO)_2$] at 1839 and 1761 cm^{-1} as well as an increase in the MS intensity of N_2O and $m/e = 28$. CO_2 was not produced during the pulse, indicating the absence of the reaction between $Rh^+(CO)_2$ and gaseous NO. The absence of the reaction was further verified (not shown here) by the exposure of $Rh^+(CO)_2$ to various NO pulse sizes ranging from 0.5 to 10 cm^3 on 2 wt% Rh/Al_2O_3 and 0.2 wt% Rh/Al_2O_3 catalysts. The lack of reactivity of $Rh^+(CO)_2$ toward gaseous NO could be due to the absence of Rh^0 sites for NO dissociation and the insufficient concentration of Rh–NO^- during the NO pulse over $Rh^+(CO)_2$.

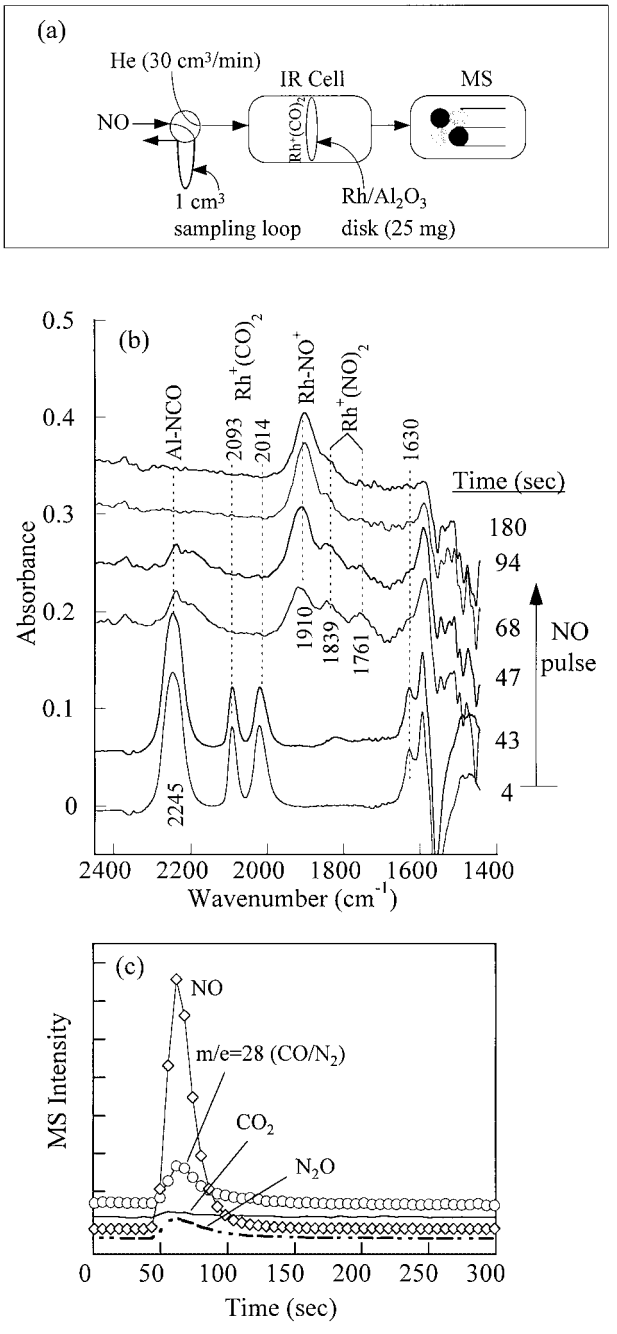

FIG. 1. (a) Experimental approach: pulsing 1 cm^3 of NO over $Rh^+(CO)_2$, (b) IR spectra collected during a 1-cm^3 NO pulse over 2 wt% Rh/Al_2O_3 at 573 K, and (c) MS analysis of the reactor effluent.

Reaction of $Rh^+(CO)_2$ with $^{13}CO/NO$

The presence of CO along with NO could promote the reduction of Rh^+ to Rh^0, facilitating NO dissociation and CO_2 formation. The presence of both NO and CO reactants may be needed to activate $Rh^+(CO)_2$ for the reaction with NO. Pulsing 10 cm^3 of $^{13}CO/NO$ at a molar ratio of 1:1 was carried out over 2 wt% Rh/Al_2O_3 and 0.2 wt%

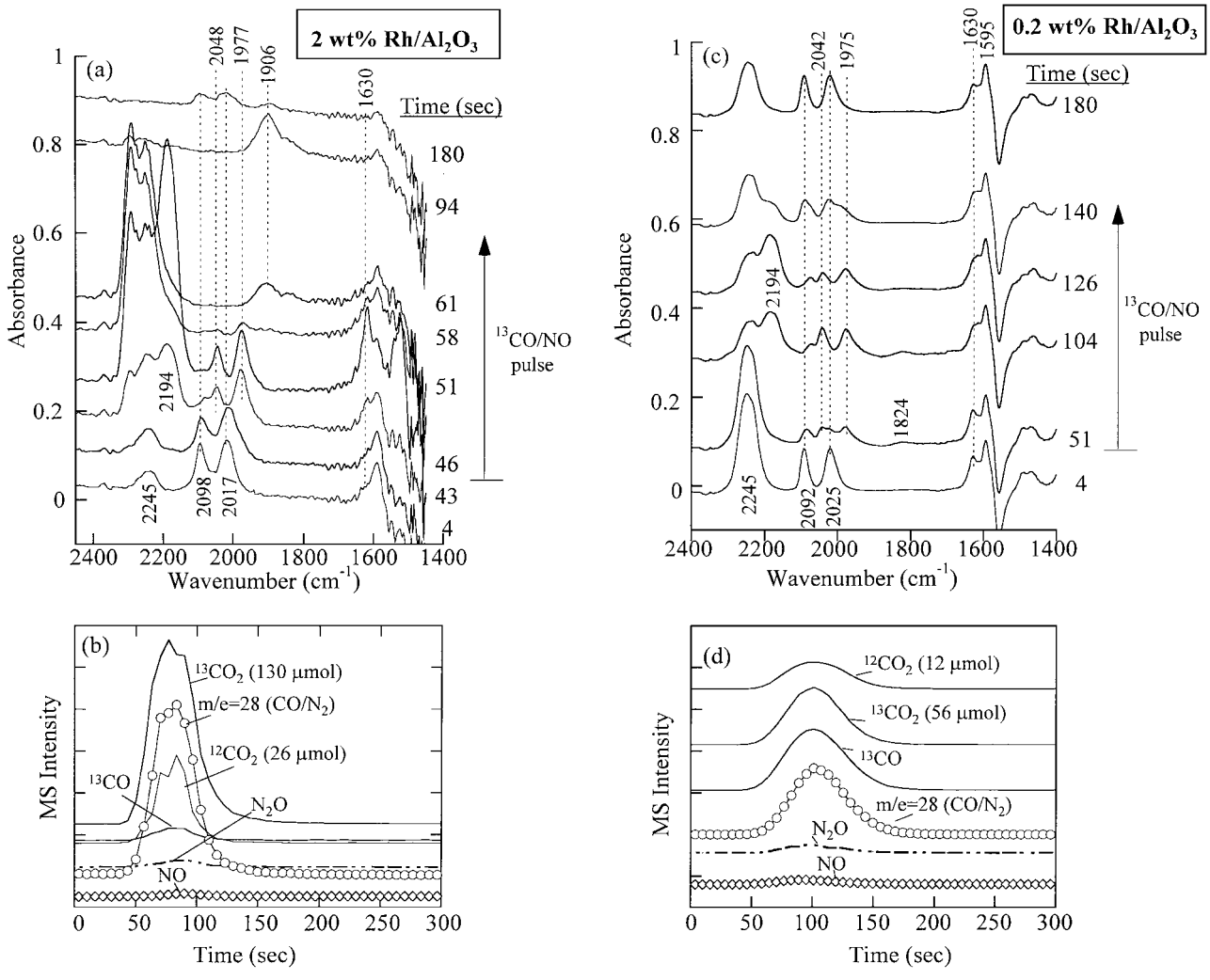

FIG. 2. (a) IR spectra collected during a 10-cm^3 $^{13}CO/NO$ pulse at a molar ratio of 1 : 1 over 2 wt% Rh/Al_2O_3 at 573 K and (b) MS analysis of the reactor effluent. (c) IR spectra collected during a 10 cm^3 $^{13}CO/NO$ pulse at a molar ratio of 1 : 1 over 0.2 wt% Rh/Al_2O_3 at 573 K and (d) MS analysis of the reactor effluent.

Rh/Al_2O_3 at 573 K to determine $Rh^+(CO)_2$ reactivity in the presence of gaseous NO and CO. Investigation of two different Rh loadings allowed the determination of the Rh particle size effects on the $Rh^+(CO)_2$ reactivity and verification of the IR and MS observations. Figure 2a shows that pulsing $^{13}CO/NO$ over $Rh^+(^{12}CO)_2$ at 2098 and 2017 cm^{-1} caused the disappearance of $Rh^+(^{12}CO)_2$ and the formation of $Rh^+(^{13}CO)_2$ at 2048 and 1977 cm^{-1} and Rh^0–NO^- at 1630 cm^{-1}. Figure 2b shows that the pulse produced $^{13}CO_2$ and $^{12}CO_2$ and achieved nearly complete NO conversion. Although $^{12}CO_2$ can be formed from the reaction of gaseous ^{12}CO desorbed from $Rh^+(^{12}CO)_2$, the close relationship between the decrease in $Rh^+(^{12}CO)_2$ intensity and the increase in $^{12}CO_2$ formation suggests that $^{12}CO_2$ formation is a result of the reaction between $Rh^+(^{12}CO)_2$ and adsorbed oxygen from dissociated NO.

The dramatic enhancement of $Rh^+(CO)_2$ reactivity in the presence of both NO and CO could be due to not only CO-induced reductive agglomeration of Rh^+ to Rh^0 crystallites but also high CO coverage. The former is evidenced by a significantly higher intensity of the band at 1997 cm^{-1} than that at 2048 cm^{-1} (shown in Fig. 2a), indicating that the Rh^0–^{13}CO band produced from reductive agglomeration is overlapped with the asymmetric component of $Rh^+(^{13}CO)_2$. The formation of Rh^0 is further evidenced by the presence of Rh^0–NO^- at 1630 cm^{-1}.

The intensity of $Rh^+(^{12}CO)_2$ is approximately the same (i.e., an equal amount of $Rh^+(^{12}CO)_2$ species) for both 2 wt% Rh/Al_2O_3 and 0.2 wt% Rh/Al_2O_3 catalysts as shown in Figs. 2a and 2c; however, Figs. 2b and 2d show that the 2 wt% Rh/Al_2O_3 produced more $^{12}CO_2$ and $^{13}CO_2$ as well as higher NO conversion than 0.2 wt% Rh/Al_2O_3. This high

activity of the 2 wt% Rh/Al_2O_3 catalyst may be attributed to its large, reduced Rh^0 crystallites. The hydrogen chemisorption study shows that the 2 wt% Rh/Al_2O_3 catalyst has an average Rh crystallite size of 52 Å whereas 0.2 wt% Rh/Al_2O_3 is highly dispersed with a Rh crystallite size of 11 Å. The relationship between the NO–CO reaction activity and the Rh crystallite size has also been established for Rh/Al_2O_3 and shows that the catalyst activity for the reaction increased with increasing Rh crystallite size (36).

Reaction of $Rh^+(CO)_2$ with NO/H_2

To further elucidate the role of reducing agents in CO_2 formation, $Rh^+(CO)_2$ was exposed to an NO/H_2 pulse. Pulsing 0.5 cm^3 of NO/H_2 at a molar ratio of 1 : 1 over $Rh^+(CO)_2$ on 0.2 wt% Rh/Al_2O_3 at 573 K as shown in Figs. 3a and 3b caused (i) a decrease in Al–NCO at 2237 cm^{-1}, (ii) a decrease in the band at 2091 cm^{-1} and an increase in the band at 2020 cm^{-1}, and (iii) N_2O formation. A decrease in $Rh^+(CO)_2$ would cause an intensity reduction in both bands at 2091 and 2020 cm^{-1} while an increase in Rh^0–CO would increase the band intensity in the 2010- to 2060-cm^{-1} region. Variation of the bands at 2091 and 2002 cm^{-1} can be further highlighted by the difference spectra presented in the inset in Fig. 3a which shows a negative band at 2091 cm^{-1} as well as positive bands at 2002 and 3735 cm^{-1}. The negative band at 2091 cm^{-1} reflects a decrease in the $Rh^+(CO)_2$ concentration while positive bands at 2020 and 3735 cm^{-1} correspond to an increase in the concentration of Rh^0–CO and an isolated OH group, respectively. The variation of these species in the presence of H_2 has been attributed to the following reaction (8),

$$\tfrac{1}{2}H_2(g) + Rh^+CO_2 \rightleftarrows Rh^0\text{–}CO + OH + CO(g),$$

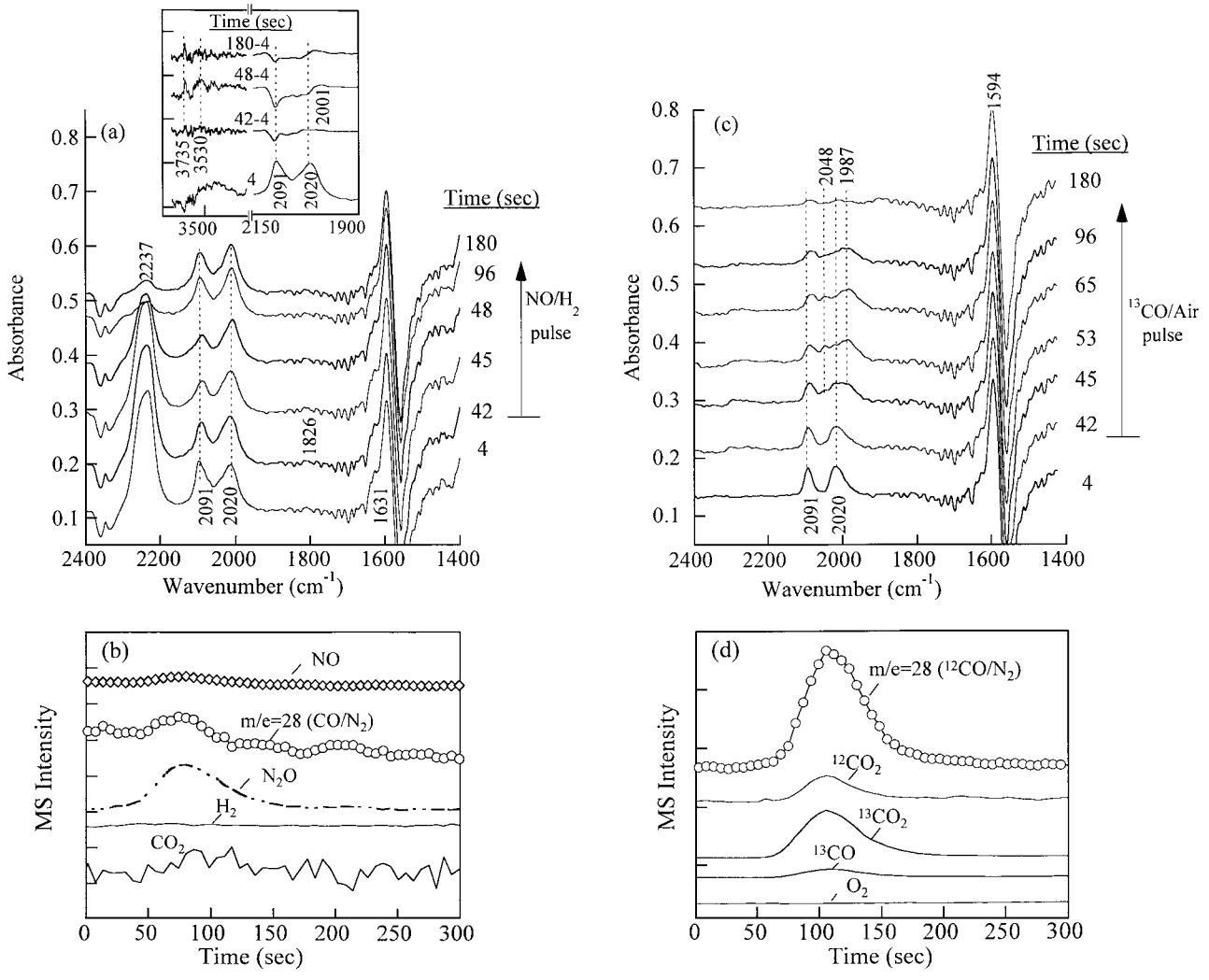

FIG. 3. (a) IR spectra collected during a 0.5-cm^3 $^{13}CO/H_2$ pulse at a molar ratio of 1 : 1 over 0.2 wt% Rh/Al_2O_3 at 573 K and (b) MS analysis of the reactor effluent. (c) IR spectra collected during a 0.5 cm^3 ^{13}CO/air pulse at a molar ratio of 1 : 1 over 0.2 wt% Rh/Al_2O_3 at 573 K and (d) MS analysis of the reactor effluent.

which indicates conversion of Rh^+ to Rh^0 sites and $Rh^+(CO)_2$ to Rh^0–CO.

Although the presence of H_2 reduces part of Rh^+ to Rh^0 for NO dissociation, $Rh^+(CO)_2$ remains inactive toward gaseous NO. Adsorbed oxygen from dissociated NO is unable to access adsorbed CO (i.e., $Rh^+(CO)_2$ and Rh^0–CO) for CO_2 formation. We speculate that the concentration of Rh^0 sites produced from H_2-induced reductive agglomeration is too low and these sites are too far away from the CO sites to react with CO and produce CO_2. Thus, we postulate that a sufficiently high concentration of both Rh^0 and Rh^+ as well as both the adsorbed reductant and oxidant may be needed to initiate and sustain the NO–CO redox reaction cycle as shown in Fig. 4b. In this cycle, Rh^0–NO^- dissociates to produce N_2 and Rh^+ sites (step 3) for $Rh^+(CO)_2$ formation (step 4); CO reduces Rh^+ to Rh^0 (step 5), leading to CO_2 formation. CO-induced reductive agglomeration (i.e., step 5) has been well-established (3, 5, 7, 19). Our postulation is supported by the results of a $^{13}CO/NO$ pulse over $Rh^+(CO)_2$ on which CO promotes reduction of Rh^+ to Rh^0 sites for Rh^0–NO^- adsorption and dissociation.

Reaction of $Rh^+(CO)_2$ with Air and ^{13}CO/Air

Since CO in $Rh^+(CO)_2$ was not accessible for the reaction with adsorbed oxygen from dissociated NO during the NO/H_2 pulse, the reactivity of $Rh^+(CO)_2$ toward adsorbed oxygen was further investigated by pulsing air and ^{13}CO/air over $Rh^+(CO)_2$ on 0.2 wt% Rh/Al_2O_3. Pulsing 0.5 or 10 cm^3 of air over $Rh^+(CO)_2$ (not shown here) did not cause any variation in the $Rh^+(CO)_2$ intensity and did not produce CO_2 as well. Lack of reactivity of $Rh^+(CO)_2$ toward gaseous O_2 has also been reported on Rh/SiO_2 (10).

Addition of ^{13}CO to air for the pulse dramatically modified the reactivity of $Rh^+(CO)_2$ toward oxygen. Figures 3c and 3d show that pulsing 0.5 cm^3 of ^{13}CO/air at a molar ratio

(a) Proposed mechanism of the NO-CO reaction

Step 1	Rh^0	+	$CO_{(g)}$	$\rightleftharpoons$	Rh^0-CO			
Step 2	Rh^0	+	$NO_{(g)}$	$\rightleftharpoons$	Rh^0-NO^-			
Step 3	Rh^0-NO^-	+	Rh^0	$\rightleftharpoons$	$(Rh^+)_2O^{2-}$	+	$\frac{1}{2}N_2$	
Step 4	$(Rh^+)_2O^{2-}$	+	$4CO_{(g)}$	$\rightleftharpoons$	2 $Rh^+(CO)_2$	+	O^{2-}	
Step 5	2 $Rh^+(CO)_2$	+	O^{2-}	$\overset{CO_{(g)}}{\rightleftharpoons}$	2 Rh^0-CO	+	$CO_{2(g)}$ + $CO_{(g)}$	
Step 6	$Rh^+(CO)_2$	+	$NO_{(g)}$	$\rightleftharpoons$	Rh-NO^+	+	2 $CO_{(g)}$	
Step 7	Rh^0-CO	+	$NO_{(g)}$	$\rightleftharpoons$	Rh^0-NO^-	+	$CO_{(g)}$	

(b) Steps involved in the NO-CO redox cycle

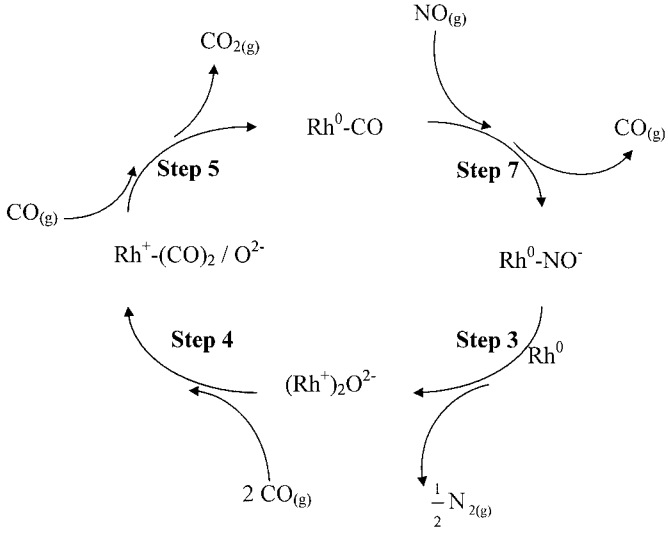

FIG. 4. (a) Proposed mechanism of the NO–CO reaction and (b) steps involved in the NO–CO redox reaction cycle.

of 1 : 1 over $Rh^+(CO)_2$ at 573 K caused the disappearance of $Rh^+(^{12}CO)_2$ at 2091 and 2020 cm^{-1}, the appearance of $Rh^+(^{13}CO)_2$ at 2048 and 1987 cm^{-1}, and $^{12}CO_2/^{13}CO_2$ formation. The significant broadening of the band in the 1950- to 2070-cm^{-1} region indicates the formation of Rh^0–^{12}CO and Rh^0–^{13}CO species during the ^{13}CO/air pulse. Depletion of $Rh^+(^{12}CO)_2$ and formation of Rh^0–^{12}CO, Rh^0–^{13}CO, and $^{12}CO_2$ clearly indicates that the presence of gaseous ^{13}CO promotes the formation of Rh^0 sites, facilitating the reaction between $Rh^+(^{12}CO)_2$ and adsorbed oxygen to form $^{12}CO_2$.

CONCLUSIONS

Sufficiently high concentrations of both Rh^0 and Rh^+ as well as both the adsorbed reductant and oxidant are needed to initiate and sustain the redox cycle of the NO–CO and CO–O_2 reactions on the Rh catalyst. Results of this study suggest that the reactivity of adsorbates can only be reliably measured under conditions where all the reactants are present on the catalyst. Studies involving exposure of the first reactant adsorbate to the second or third reactant may not provide information directly relevant to heterogeneous catalysis of redox reactions.

ACKNOWLEDGMENT

The authors gratefully acknowledge the support of this research by the National Science Foundation under Grant CTS-942111996.

REFERENCES

1. Yang, A. C., and Garland, C. W., *J. Phys. Chem*. **61**, 1504 (1957).
2. Yates, J. T., Jr., Duncan, T. M., Worley, S. D., and Vaughan, R. W., *J. Chem. Phys*. **70**, 1219 (1979).
3. Solymosi, F., and Rasko, J., *J. Catal*. **63**, 217 (1980).
4. Hecker, W. C., and Bell, A. T., *J. Catal*. **84**, 200 (1983).
5. Solymosi, F., and Pasztor, M., *J. Phys. Chem*. **89**, 4789 (1985).
6. Wong, C., and McCabe, R. W., *J. Catal*. **107**, 535 (1987).
7. Solymosi, F., Bansagi, T., and Novak, E., *J. Catal*. **112**, 183 (1988).
8. Basu, P., Panayotov, D., and Yates, J. T., Jr., *J. Am. Chem. Soc*. **110**, 2074 (1988).
9. Dictor, R., *J. Catal*. **109**, 89 (1988).
10. Li, Y. E., and Gonzalez, R. D., *J. Phys. Chem*. **92**, 1589 (1988).
11. Buchanan, D. A., Hemandez, M. E., Solymosi, F., and Whit, J. M., *J. Catal*. **125**, 456 (1990).
12. Paul, D. K., and Yates, J. T., Jr., *J. Phys. Chem*. **95**, 1699 (1991).
13. Logan, A. D., Sharoudi, K., and Datye, A. K., *J. Phys. Chem*. **95**, 5568 (1991).
14. Anderson, J. A., *J. Chem. Soc., Faraday Trans*. **87**, 3907 (1991).
15. Chuang, S. S. C., and Pien, S. I., *J. Catal*. **135**, 618 (1992).
16. Srinivas, G., Chuang, S. S. C., and Debnath, S., *J. Catal*. **148**, 748 (1994).
17. Krishnamurthy, R., and Chuang, S. S. C., *J. Phys. Chem*. **99**, 16727 (1995).
18. Berko, A., Menesi, G., and Solymosi, F., *J. Phys. Chem. B* **100**, 17732 (1996).
19. Novak, E., Sprinceana, D., and Solymosi, F., *Appl. Catal. A* **149**, 89 (1997).
20. Conners, L., Hollis, T., Johnson, D. A., and Blyholder, G., *J. Phys. Chem. B* **102**, 10112 (1998).
21. Oh, S. H., Fisher, G. B., Carpenter, J. E., and Goodman, D. W., *J. Catal*. **100**, 360 (1986).
22. Cho, B. K., Shanks, B. H., and Bailey, J. E., *J. Catal*. **109**, 89 (1989).
23. Taylor, K. C., *Catal. Rev.-Sci. Eng*. **35**, 457 (1993).
24. Shelef, M., *Catal. Rev.-Sci. Eng*. **36**, 443 (1994).
25. Simon Ng, K. Y., Belton, D. N., Schmieg, S. J., and Fisher, G. B., *J. Catal*. **146**, 394 (1994).
26. Lamb, H. H., Gates, B. C., and Knozinger, H., *Angew. Chem., Int. Ed. Engl*. **27**, 1127 (1988).
27. Ichikawa, M., *in* "Advances in Catalysis," Vol. 38, p. 283. Academic Press, New York, 1992.
28. Chuang, S. S. C., and Debnath, S., *J. Mol. Catal*. **79**, 323 (1993).
29. Srinivas, G., and Chuang, S. S. C., *J. Phys. Chem*. **98**, 3031 (1994).
30. Chuang, S. S. C., Srinivas, G., and Mukherjee, A., *J. Catal*. **139**, 490 (1993).
31. Krishnamurthy, R., Chuang, S. S. C., and Balakos, M. W., *J. Catal*. **157**, 512 (1995).
32. Chuang, S. S. C., and Tan, C. D., *J. Catal*. **173**, 104 (1998).
33. Almusaiteer, A. K., and Chuang, S. S. C., *J. Catal*. **180**, 161 (1998).
34. Chuang, S. S. C., Brundage, M. A., Balakos, M. W., and Srinivas, G., *Appl. Spectrosc*. **49**, 1151 (1995).
35. Almusaiteer, K., Ph.D. Dissertation, University of Akron, Akron, OH, 1999.
36. Oh, S. H., and Eickel, C. C., *J. Catal*. **128**, 526 (1991).